CAVITATION BUBBLE OBSERVATIONS IN A VENTURI

R. D. Ivany

F. G. Hammitt

Internal Report 03424-25-I
(Submitted for ASME Paper)

April, 1965

Laboratory for Fluid Flow and Heat Transport Phenomena

Nuclear Engineering Department

University of Michigan

Support by NASA Grant NsG-39-60

and NSF Grant G-22529

[redacted]

TABLE OF CONTENTS

ABSTRACT

Bubbles collapsing in water in a cavitating venturi are photographically observed. The large pressure gradient in the venturi causes the bubbles to collapse by flattening in the direction of flow. A comparison of observed collapse rates with incompressible theory for a spherical bubble indicates that the observed slowing down of collapse at small bubble radii may result from compression of vapor within the bubble.

ACKNOWLEDGEMENTS

The financial support of grants from the National Aeronautics and Space Administration and from the National Science Foundation in this work is appreciated.

LIST OF FIGURES

NOMENCLATURE

c_p	Specific Heat Liquid
L	Latent Heat
p_∞	Liquid Pressure Away From Bubble
p_v	Vapor Pressure
p_o	Pressure Inside Bubble
R	Bubble Radius
R_o	Initial or Maximum Bubble Radius
t	Time
T_{sat}	Liquid Saturation Temperature
T_{liq}	Liquid Temperature
U	Bubble Wall Radial Velocity
B	Thermodynamic Parameter
Ja	Jakob Number
B_{eff}, B_{sat}, C	Dimensionless Parameters
σ	Surface Tension
μ	Liquid Shear Viscosity
α	Liquid Thermal Diffusivity
ρ_L	Liquid Density

I. INTRODUCTION

Analyses of the growth and collapse of cavitation bubbles usually consider that they exist in an infinite sea of fluid which is initially at uniform and constant pressure. Many such analyses, of increasing complexity as more realistic fluid parameters are considered, are in the literature, including a recent one by the present authors.[1] Actually, cavitation bubbles as they exist in fluid-handling machinery or in most test devices, grow and collapse in non-uniform, time-varying pressure fields, and often in close proximity to other bubbles and structures. Observations on bubble growth and collapse in a cavitating venturi, wherein the external pressure seen by the bubble is highly time-varying, and is non-symmetrical with respect to the bubble, and where the bubbles are sometimes very substantially influenced by other bubbles and by the surrounding structure, are herein reported. The rates of collapse and growth are compared to those computed[1] for isolated spherical bubbles in a spherically-symmetric, though time-varying, pressure field. In addition measurements and prediction of bubble "slip" in this flow regime are discussed.

II. PRESSURE ENVIRONMENT OF BUBBLE IN VENTURI

Cavitation bubbles in fluid-machinery typically grow in a low pressure region, are convected into a higher pressure region, whereupon they collapse, frequently with accompanying

pitting of adjacent solid material. To observe bubble behavior as a function of the surrounding pressure, a two-dimensional, plexiglas cavitating venturi was used for this work. The bubbles were observed photographically, and the corresponding pressure distributions measured.

The overall facility has been described previously[2]. However, some of the significant features are summarized here for convenience. The venturi is installed in a closed loop driven by a variable-speed centrifugal pump. This provides water flow to a high-pressure manifold from which four parallel piping systems connect to a low-pressure manifold from which the pump takes suction. In each loop a test venturi can be installed, and all loops can be operated simultaneously. A surge tank is connected through small-bore tubing (to prevent significant gas diffusion) to the low-pressure manifold, and the gas pressure over the water in the surge tank determines the loop reference pressure. For the present tests three of the loops were blanked-off, and the fourth loop assembled with the two-dimensional plexiglas venturi shown schematically in Fig. 1.

Associated with a given extent of cavitation in the venturi ("degree of cavitation") there are three important flow variables. The first variable, flow-rate, is determined by pump speed (there are no valves in the main loop), and measured by an orifice. For a given flow, the pressure on the surge

tank is set to give the desired degree of cavitation. In the present tests this was always the minimum necessary for good photographs. The second variable is air content which can be varied with the present equipment from slightly supersaturated to 30% of saturation (at STP). The third variable, temperature, is controlled by the balance between pump-work input and heat removal by cooling coils within the low pressure tank, which can be controlled by adjusting coolant flow.

Twelve pressure taps were placed on one of the contoured plexiglas faces of the venturi (Fig. 2). A small arrow was marked (without appreciably indenting the surface) on the inner flow surface of the venturi in the region of the constant area throat, to be used as a scale reference for the photographs. The tip of the arrow at the throat exit points in the direction of flow. A typical still photograph showing the arrow (Fig. 3) was taken with a 4" x 5" camera using a 3 micro-second flash. The degree of cavitation ("Cavitation to 0.75 inches") is the same as that used for the high-speed motion pictures to be described later. In all photographs the constant, larger venturi dimension (3 inches) is vertical. The throat opening is then $\frac{1}{4}$" x 3", and the flow is from left to right. The normalized pressure profiles for several flow conditions are shown in Fig. 4. Non-normalized profiles for similar conditions are shown in Fig. 5. The two curves shown in Fig. 5 are for the same flow rate, the only difference being an increase in the surge tank pressure by about 2.7 psi.

This causes the degree of cavitation to decrease from "cavitation to 0.75 inches" to "visible initiation".* The pressure rise corresponding to the 2.7 psi increase in surge tank pressure, 0.5 inches downstream from the throat exit is 9 psi. Thus, slight changes in reference pressure cause proportionately larger changes in the pressures just downstream of the venturi throat, i.e., the driving pressures for bubble collapse.

III. PHOTOGRAPHIC BUBBLE OBSERVATIONS

A Fastax camera at a framing rate of 7700 frames per second, synchronized with a one microsecond duration strobelight, was used for the bubble observations. Fig. 6 is a schematic of the camera arrangement, and also indicates the size of the field of view. Fig. 7, 8, and 9 are typical sequences showing bubble growth and collapse.

Fig. 7 shows a bubble rebound (into an apparently irregular mass rather than a spherical bubble) in going from frame 5 to frame 7. Fig. 8 shows the typical behavior of two bubbles, one following the other, then joining and collapsing as one. Fig. 9, e.g., frames 11 through 18, show two bubbles traveling parallel to each other apparently growing and collapsing independently, thus verifying the two-dimensional nature of the flow. Also note Frames 21 through 25 in Fig. 9. The bubble collapses in a manner typical of this flow regime according to the present observations, i.e., by drastically and suddenly flattening on the downstream side. However, in

---

* No hysteresis was noted in these tests.

frame 25 it appears that a jet has passed through the bubble in the upstream direction, thereby creating a torus-shaped void. This is similar in appearance to gas bubbles rising in a gravitational field as reported by Walters and Davidson[3], e.g., or to a collapse of a spark-generated bubble near a solid surface as shown by Naude and Ellis[4] and Shutler and Mesler[5].

A frame by frame analysis was made to obtain bubble growth-collapse curves. All the bubbles on the film which grew approximately spherically, and which did not appear to strike the venturi wall (evidenced by irregular surface and by streamers tailing from behind the bubble, see, e.g. Frame 6, Fig. 9), and had a maximum diameter greater than about 15 mils were included. There were 73 such bubbles, with a total of 597 bubble images. Four pieces of information were obtained for each image: the framing rate at that film location, the axial distance of the bubble from the throat exit in each frame, and the maximum dimensions horizontally and vertically since in some cases there was a marked departure from sphericidicity. For the non-spherical cases the void was assumed to be an ellipsoid with one axis parallel to the venturi center line. The radius for a sphere of the same volume was then recorded. The average maximum radius, R_0 was 36.5 mils and the maximum and minimum values of R_0, for bubbles which were tabulated, were 68.3 and 19.6 mils respectively.

A randomly-selected length of the film was also analyzed for total void content. The irregular, approximately stationary, masses of void were assumed attached to the walls, and

their thickness was approximated from typical still photographs taken at 90° to the motion pictures. The maximum total void as a percent of the flow area in the field photographed was 4.1 percent. However, there was considerable variation in the void fraction, with the time-average being only 0.2 percent. The liquid velocity in the throat computed from the known flow rate (the correction for the void fraction is negligible) was 74.6 ft/sec. The bubble translational velocity in the throat, and for about 0.2 inches into the diffuser portion of the venturi, was ~87 ft/sec, making the slip-ratio 1.17 (ratio of bubble to liquid velocity). That it should be $\geq$ 1.0 is expected, since in an accelerating flow in a falling pressure gradient the bubbles would be accelerated faster than the liquid because of their lower density, assuming that they feel the same pressure gradient as the liquid. In the region of the start of bubble collapse in the venturi, translational velocity of the bubbles decreases, and the slip ratio becomes about 1.0.

All 73 bubble radii are included in Fig. 10 where normalized radius is plotted vs. distance from the throat exit (positive downstream and negative upstream). The points are replotted in Fig. 11 as normalized radius vs. time from the first observed maximum radius of each bubble (some bubbles were approximately of the same size in two frames). It is seen in both figures that the bubble wall collapse velocity decreases at normalized radii below about 0.5. The triangular

points in both figures represent bubbles which rebound; the first triangle for each being the minimum bubble radius. It is observed that the bubble does not rebound into a smooth spherical bubble as it initially appeared, but rather as an irregular mass with a rough surface.

A reduction of the air content of the loop water from saturation to about 40% of saturation (computed at STP) had no apparent effect on the existence of bubble rebounds. The film taken with saturated water showed that of the 73 bubbles observed 23 percent rebounded. The film taken with reduced air content showed 19 spherical bubbles of which 9 definitely rebounded. Another 5 grew and apparently struck the wall, as evidenced by streamers trailing from the bubble, before collapsing. The irregular streamer or wake of the bubble appeared to grow larger, or rebound, but this behavior is not interpreted here to be that of a rebounding bubble. The samples observed are too small to conclude that reduction of air content actually increased the proportion of bubbles that rebounded. However, it appears clear that the rebounding proportion was not significantly reduced, as might have been expected, by the reduction in air content. There was some difference in the initial bubble appearance, however, in that bubbles in water at lower air content had a much more irregular surface than those at higher air content (Fig. 7, 8, and 9). The fact that the lower air content did not apparently inhibit bubble rebound, plus the fact that the collapse wall velocity decreases for small radii suggests that there may be substantial departure from thermal equilibrium in that the vapor within the bubble may

begin to behave as a compressed gas as the bubble wall collapse velocity increases. The maximum observed collapse velocities, i.e. taken while bubbles were large enough to be visible, were between 12 and 20 ft/sec.

The scatter of the points in Fig. 10 and 11 may be due in part to the fluctuations in loop pressure due to variations in pump speed, to high-frequency pulses which could be inherent in loop resonances, etc., and to the cavitation phenomenon itself. It was mentioned previously that small loop

reference pressure changes significantly alter the location of the pressure gradient in the venturi, and therefore the pressures causing bubble collapse could vary substantially due to the above uncontrollable and random variations.

IV. THEORETICAL BUBBLE COLLAPSE CURVES

An analysis was made of a single bubble collapsing in a static, incompressible liquid. An incompressible liquid is a good assumption here since no large velocities were observed, and hence no large collapse pressures would be predicted over the observable range of R/R_o. The collapse was also assumed to be spherically-symmetric for mathematical simplicity and in order to compare with other existing analyses, although, as has been mentioned, the actual collapse was definitely non-symmetric. The assymetric collapse is presumably caused by the severely rising pressure-gradient in which the bubble exists. In Fig. 5, the maximum pressure gradient for "cavitation to 0.75 inches" is 20 psi/inch, which, for a bubble velocity of 75 ft/sec, gives a pressure rise-rate of 1.8×10^4 psi/sec as seen by the bubbles. For the average maximum bubble diameter of 73 mils there is a maximum static pressure difference, across a distance of one bubble diameter, of 1.46 psi or 3.4 ft. head of water.

The analysis follows that of Rayleigh[6], with viscosity and surface tension included in the manner first suggested by Poritsky.[7] Actually, viscosity has little effect[1] on

bubbles such as those observed here, but is included because the computer solution was programmed for a general case. For the computation, the pressure in the liquid far from the bubble is programmed to vary in the same manner with bubble radius as does the pressure measured in the venturi. The curve drawn in Fig. 10 is used to obtain the normalized bubble radius as a function of distance from the throat exit. The corresponding pressure at that distance is then obtained from Fig. 4. A curve of normalized bubble radius vs. bubble-environment pressure above vapor pressure, i.e. $p_\infty - p_v$, was plotted, and an equation fitted to the curve. Using vapor pressure as a reference is equivalent to assuming that the vapor pressure inside the bubble remains constant. However, since there was appreciable dissolved air in the cavitating water so that some diffusion into the bubble during growth is likely, and since the bubbles probably grew from gas "nuclei", the gas pressure inside the bubble (i.e., the partial pressure due to gas rather than vapor) was assumed to increase during collapse (starting from a low initial value) inversely proportional to bubble volume to the 1.3 power.

The resultant simultaneous differential equations, which were solved numerically[8] using a Runge-Kutta procedure, are:

$$2R^3 U \frac{dU}{dR} = -2R^2 \left\{ \frac{3}{2} U^2 + \frac{[p_\infty(R) - p_0(R)]}{\rho_L} + \frac{2\sigma}{R\rho_L} + \frac{4\mu U}{\rho_L R} \right\}$$

and $$\frac{dt}{dR} = \frac{1}{u}$$

The numerical results are plotted in Fig. 11 for three different initial gas pressures. It is seen that the initial internal gas pressure must be small for the calculated curve to be consistent with the initial rapid decrease in bubble radius observed experimentally. However, the experimental points indicate a gradual decrease of the bubble wall velocity, whereas the calculated curves accelerate to a final minimum radius.

Plesset[9] has made a similar comparison for bubbles growing and collapsing along an ogive in a water tunnel, observed by Knapp and Hollander.[10] In their experiment the bubble growth velocities are generally less than collapse velocities. However, this is not the case for the present study. The rate and amount of environmental pressure rise in the liquid around the bubbles reported by Plesset is comparable to that here, as is the time for collapse to one-half the initial radius (about 0.4 milliseconds).

In a later work, Plesset[11] indicates that the maximum vapor condensation rate for a moving liquid interface, taking into account the small probability of a vapor molecule sticking to the liquid surface upon striking it, is such that a water cavitation bubble wall collapse velocity $\lesssim$ 26 ft/sec. would result in an increase in the pressure of the vapor somewhat in the manner of a compressed gas. If there were also

an interposed impurity layer on the interface as has been sometimes hypothesized (Bernd[12] and Fox and Herzfeld[13]) to explain the persistence of micro-bubbles in fluids, the effect would no doubt be enhanced. Since the presently observed bubbles collapse at about this rate, credence is lent to the hypothesis of a compressed vapor reducing the collapse rate beyond that predicted assuming the vapor pressure to remain constant.

Florschuetz and Chao[14] present an analysis and experiment for static vapor bubbles collapsing in liquid. They define several normalized parameters to delineate whether inertia or heat transfer across the bubble interface, or their combination, is the predominant collapse mechanism:

$$Ja^{*} = \text{Jakob number} = \frac{\rho_L c_p (T_{sat} - T_{liq})}{\rho_v L}$$

$$C = \frac{R_o^2 (p_\infty - p_v)}{\rho_L \alpha^2}$$

Several modifications were applied to these parameters to take account of certain real fluid property variations. Using the above quantities, the parameter $B_{sat} = Ja^2/\sqrt{C}$ was defined and corrections to this value of B resulted in a quantity B_{eff} such that B_{eff} is always larger than B_{sat}. For values of $B_{eff} > 10$, Florschuetz and Chao concluded liquid

---

* Note the similarity to the Thermodynamic Parameter, B, which appears frequently in the cavitation literature, suggested initially by Stahl and Stepanoff (15) and defined in our own usage[16] as: $Ja \Big/ \frac{(p_{sat} - p_{liq})}{\rho_L}$

inertia should be predominant during collapse. The value of B_{sat} for the venturi in the present investigation was calculated using the average pressure from Fig. 5 at the location where the bubble collapsed most rapidly as determined from Fig. 10 The value of B_{sat} thus calculated was 28.9, and if appropriate corrections are made to obtain B_{eff} it would be even larger. Therefore, using the criteria of Florschuetz and Chao,[14]* the bubble collapse in the venturi should be completely controlled by liquid inertia,** However, the experimental data (Fig. 11) appear consistent with theoretical curves[14] presented for cases controlled, at least partially, by heat transfer effects. This also can be taken as supporting evidence to the hypothesis that non-equilibrium vapor compression effects are, at least partially, responsible for the retardation of collapse velocity beyond the theoretical expectation.

Finally, it has been noted that in a great many cases the collapse is non-symmetrical even within the easily visible range. While it cannot be stated at the present time as definitely proven, it seems likely that departure from spherical symmetry would reduce the collapse velocities.

---

* The motion of the bubbles relative to the liquid in the present case, compared to the static bubbles of Florschuetz & Chao, should enhance heat transfer from the bubble, thus further strengthening the conclusion that inertial effects control.

** This is in agreement with much experimentation in the cavitation field which has always shown that "thermodynamic effects" with cold water are very slight as far as gross flow parameters or component performanceare concerned.[17 e.g.]

V. CONCLUSION

Bubble collapse in the present venturi is very asymmetric and the observed collapse velocities are less than would be expected theoretically. The asymmetry of collapse may partially prevent the rapid collapse predicted. Also, a departure from thermal equilibrium at the bubble interface may contribute to the slower collapse. Observed bubble wall velocities are sufficient for this to be plausible. Other analyses[14] indicate that bubbles in such a sub-cooled environment will collapse in a manner completely determined by liquid inertia. Bubble rebounds were observed, with approximately unaffected probability over the gas content range available, i.e., from somewhat supersaturated at STP to about 40% saturation at STP. Thus, at least over the range of this experiment, gas content apparently does not influence the likelihood of rebound.

REFERENCES

1. Ivany, R. D., Hammitt, F. G., "Cavitation Bubble Collapse in Viscous, Compressible Liquids - Numerical Analyses", presented at June, 1965 ASME Conference, to be published Trans. ASME, J. Basic Engr.

2. Hammitt, F. G., "Cavitation Damage and Performance Research Facilities", ASME Symposium on Cavitation Research Facilities and Techniques, May, 1964, pp. 175-184.

3. Walters, J. K. and Davidson, J. F., "The Initial Motion of a Gas Bubble Formed in an Inviscid Liquid, Part 2, The Three Dimensional Bubble and the Toroidal Bubble", J. Fluid Mech., 17 (1963) 321-336.

4. Naudè, C. F., and Ellis, A. T., "On the Mechanism of Cavitation Damage by Nonhemispherical Cavities Collapsing in Contact with a Solid Boundary", Trans. ASME, J. Basic Eng., Series D, 83 (1961) 648-656.

5. Shutler, N. D. and Mesler, R. B., A Photographic Study of the Dynamics and Damage Capabilities of Bubbles Collapsing Near Solid Boundaries, Dept. of Chem. and Petrol. Eng., Univ. of Kansas, 1964

6. Lord Rayleigh, "On the Pressure Developed in a Liquid During the Collapse of a Spherical Cavity", Phil. Mag., 34 , (1917) 94-98.

7. Poritsky, H., "The Collapse or Growth of a Spherical Bubble or Cavity in a Viscous Fluid", Proc. First Nat'l. Congress Appl. Mech., ASME, (1952) 823-825.

8. Ivany, R. D., "Collapse of a Cavitation Bubble in Viscous, Compressible Liquid-Numerical and Experimental Analyses", Ph.D. Thesis, University of Mich., Dept. Nuc. Eng., 1965.

9. Plesset, M. S., "The Dynamics of Cavitation Bubbles", Trans. ASME, Jour. Appl. Mech., (Sept., 1949) 277-282.

10. Knapp, R. T. and Hollander, A., "Laboratory Investigations of the Mechanism of Cavitation", Trans. ASME, 70 (1948) 419.

11. Plesset, M. S., Bubble Dynamics, Report No. 85-23, Calif. Inst. Tech., 1963.

12. Bernd, L. H., "Study of the Surface Films of Gas Nuclei (as Related to Cavitation and Tensile Strength in Water)", Report TIS 64GL143, General Electric Co., Schenectady, New York, (Sept., 1964).

13. Fox, F. E. and Herzfeld, K. F., "Gas Bubbles with Organic Skin as Cavitation Nuclei", J. Acous. Soc. America, 26, No. 6, 1954.

14. Florschuetz, L. W. and Chao, B. T., "On the Mechanics of Vapor Bubble Collapse - A Theoretical and Experimental Investigation", ASME Paper No. 64-HT-23.

15. Stahl, H. A. and Stepanoff, A. J., "Thermodynamic Aspects of Cavitation in Centrifugal Pumps", Trans ASME, Vol. 78, (1956) 1691-1693.

16. Hammitt, F. G., "Liquid-Metal Cavitation-Problems and Desired Research", ASME Paper 60-HYD-13, March, 1960.

17. Hammitt, F. G., "Observations of Cavitation Scale and Thermodynamic Effects in Stationary and Rotating Components", Trans. ASME, Series D, Jour. Basic. Eng., Vol. 85, (1963) 1-12.

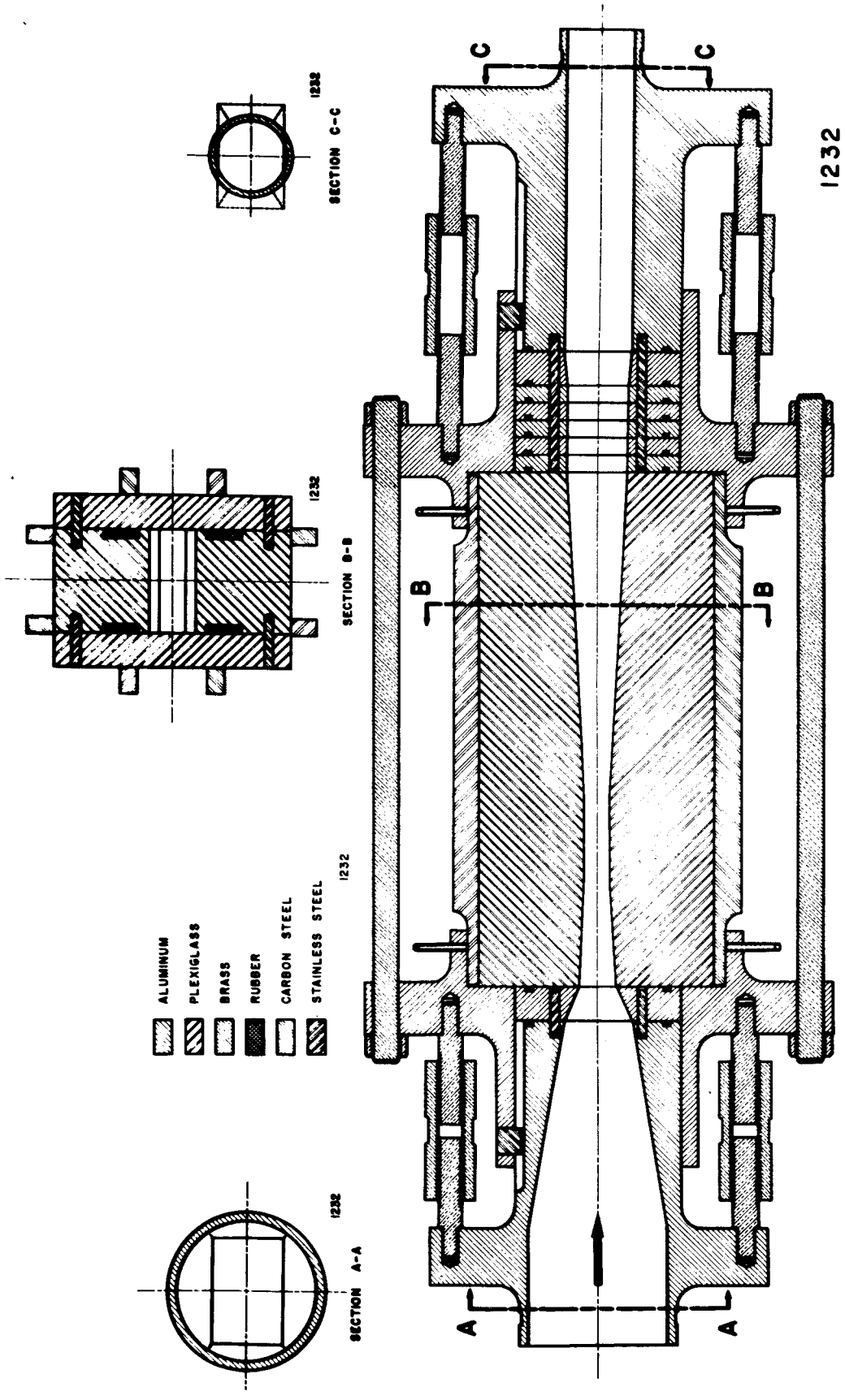

Figure 1. Schematic of Two-Dimensional Venturi

2-D Venturi Pressure Taps

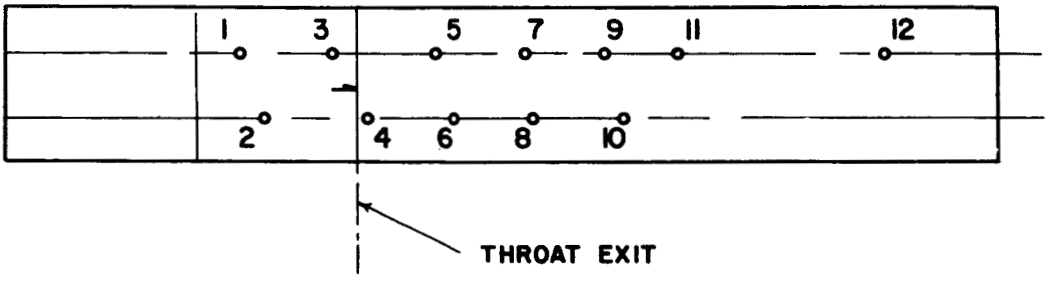

TAP #	DIST. FROM THROAT EXIT (in.)
1	− 1.030
2	− 0.654
3	− 0.275
4	+ 0.035
5	0.568
6	0.942
7	1.321
8	1.689
9	2.062
10	2.439
11	2.814
12	5.060

ARROW SIZE

1544

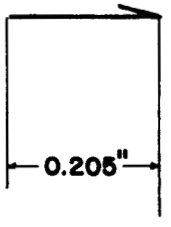

Figure 2. Locations of Pressure Taps and Scribed Arrow in Venturi

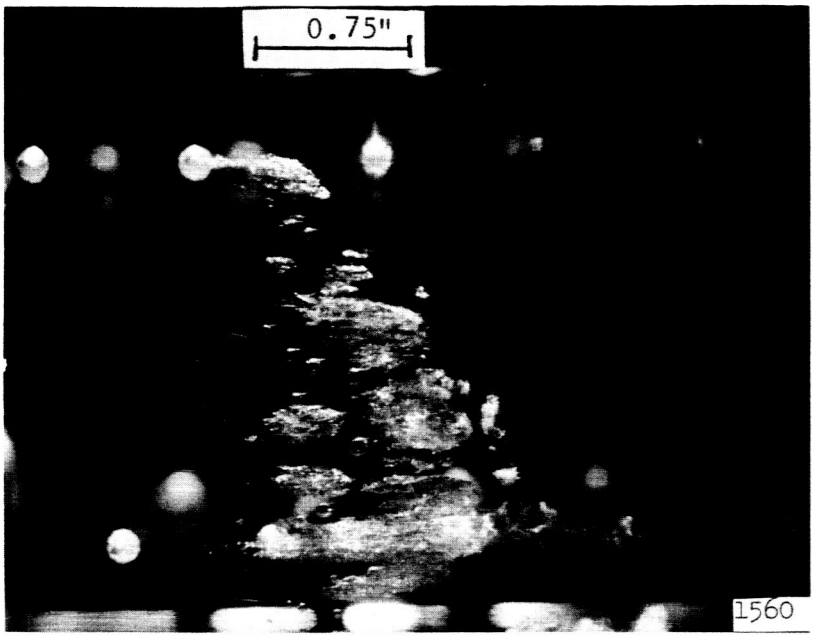

Figure 3. Still Photograph, 3 microsecond Exposure, 81.4 ft/sec, 2.05% Air Content by Volume, 68.8°F. Arrow is 0.205" Long and Tip is at Throat Exit

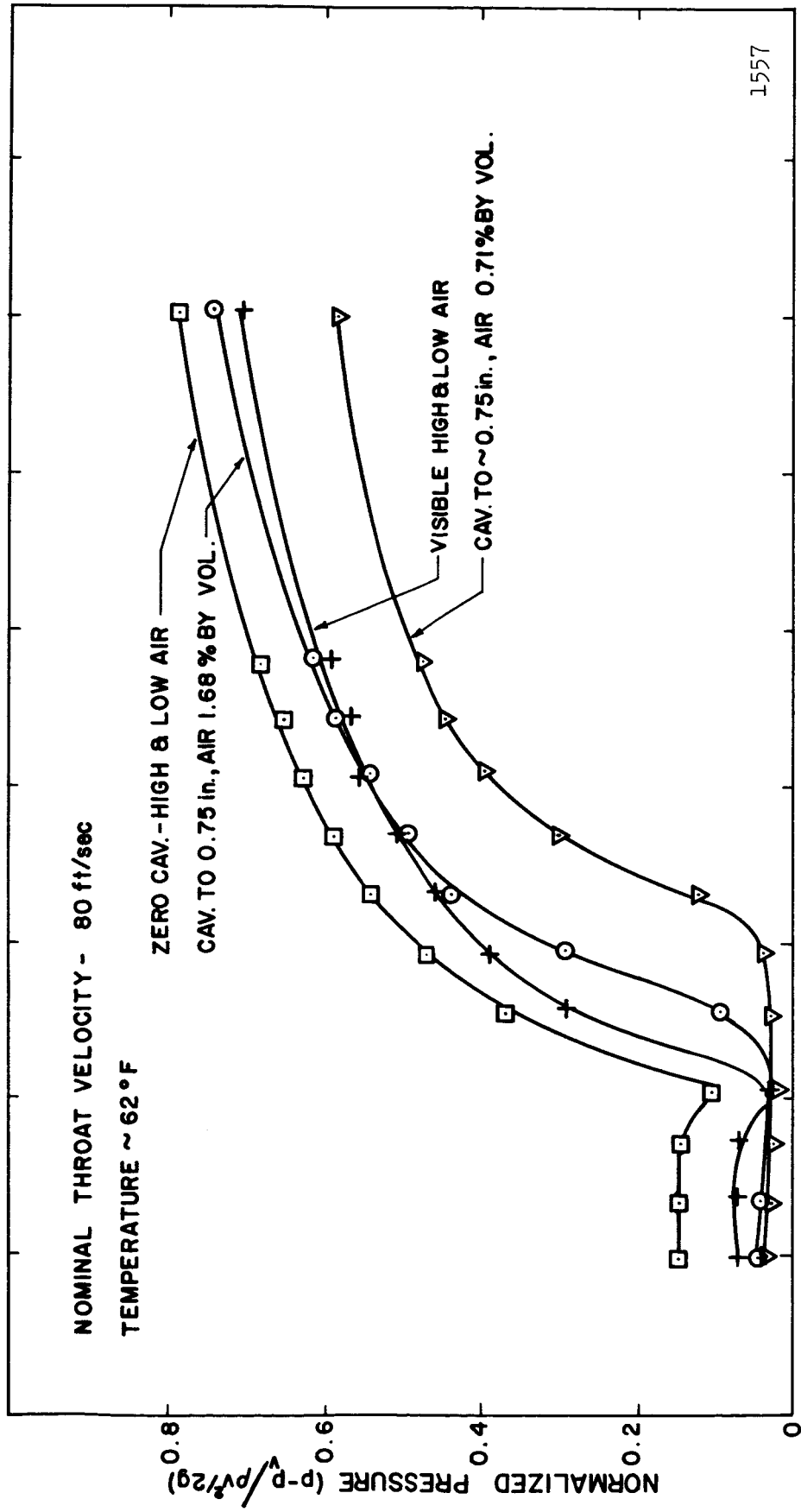

Figure 4. Normalized Pressure vs Distance from Throat Exit

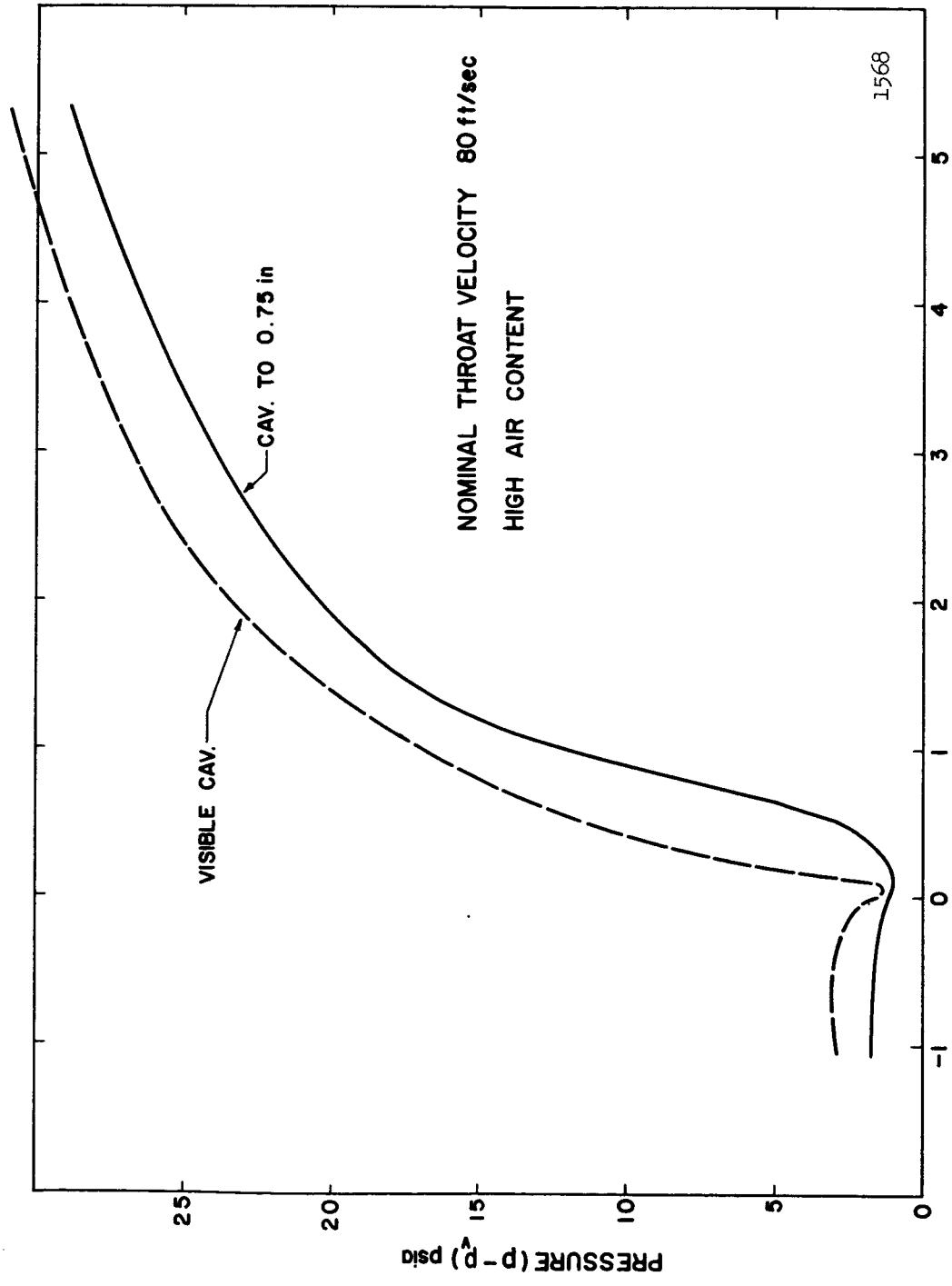

Figure 5. Pressure Above Vapor Pressure vs Distance from Throat Exit

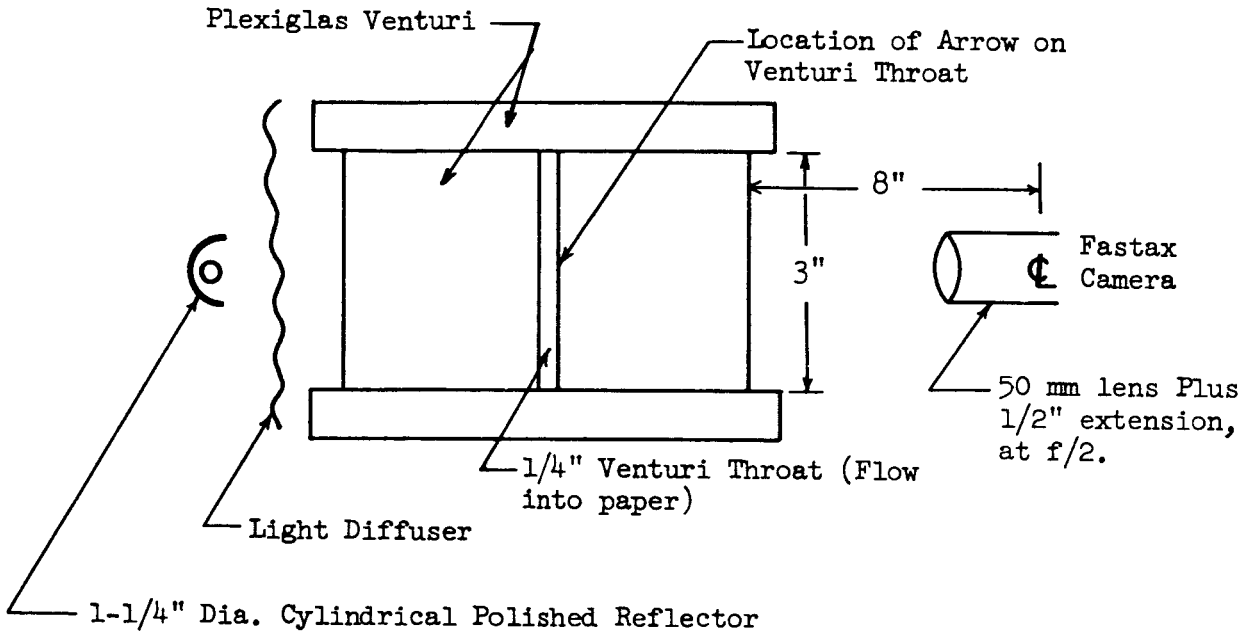

Arrangement for High Speed Photography

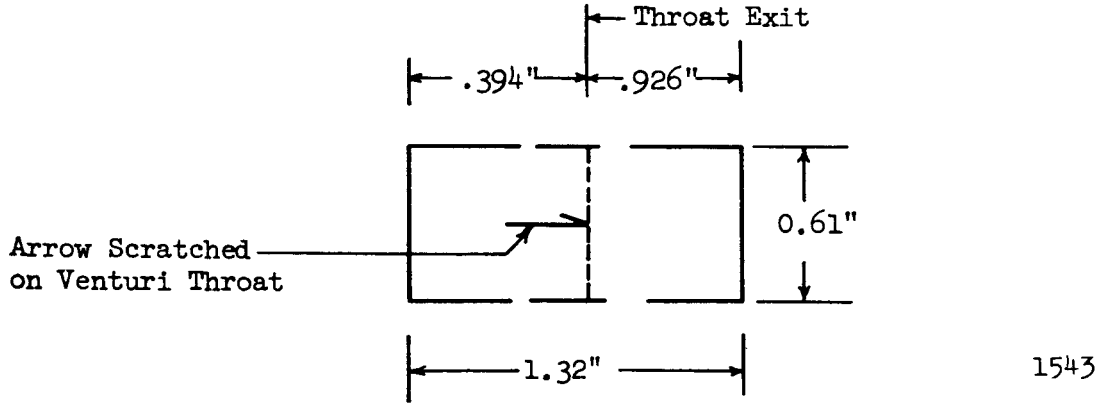

Field of View with Above Arrangement

Figure 6. Schematic Arrangement of Venturi, Camera, and Strobe Light, and Field of View Photographed

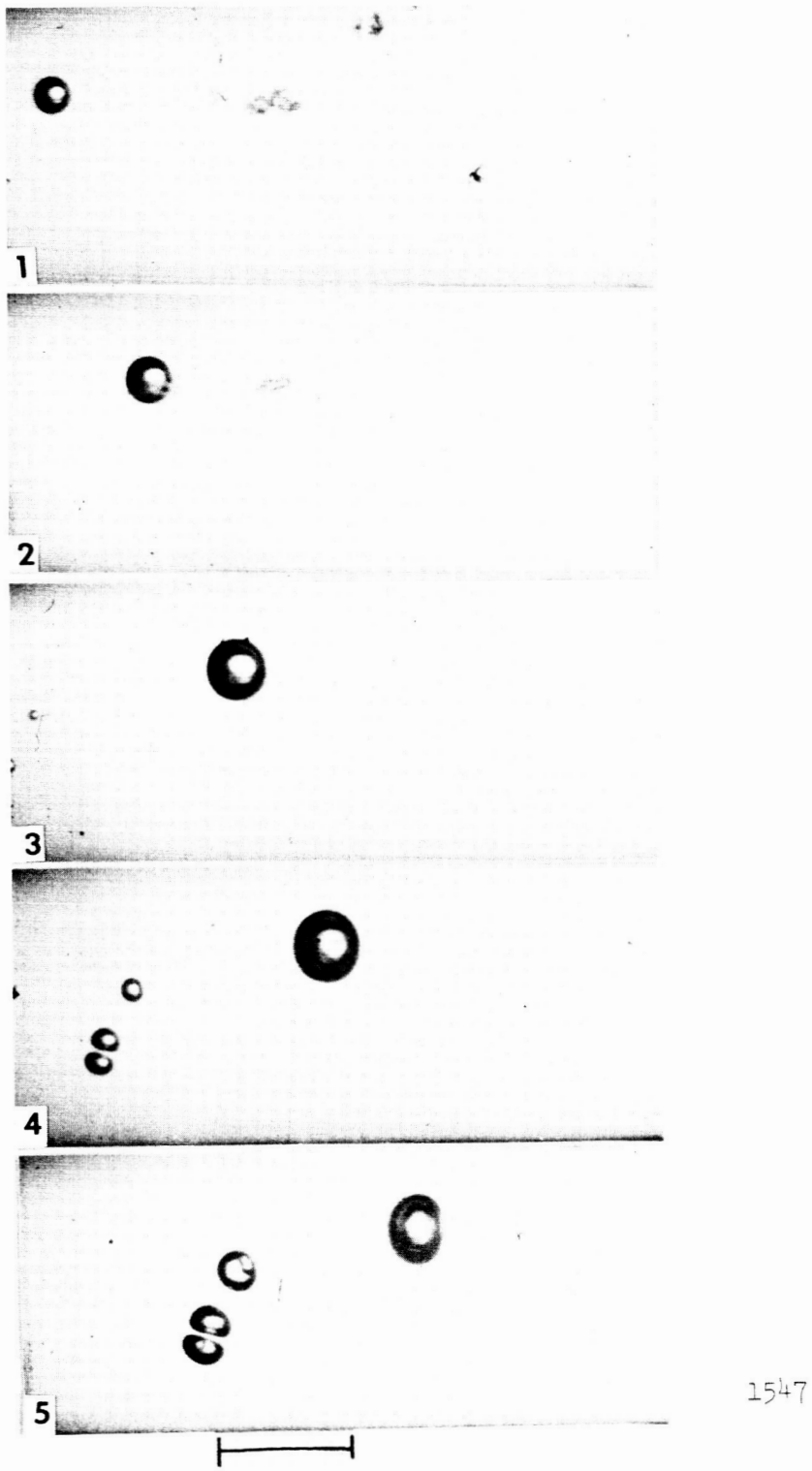

Figure 7. High Speed Photographs, 1/4 inch Venturi Throat, Velocity 74.6 ft/sec, Air Content 2.35 vol. %, 157 Microseconds per Frame, Scale Length 0.25 in.

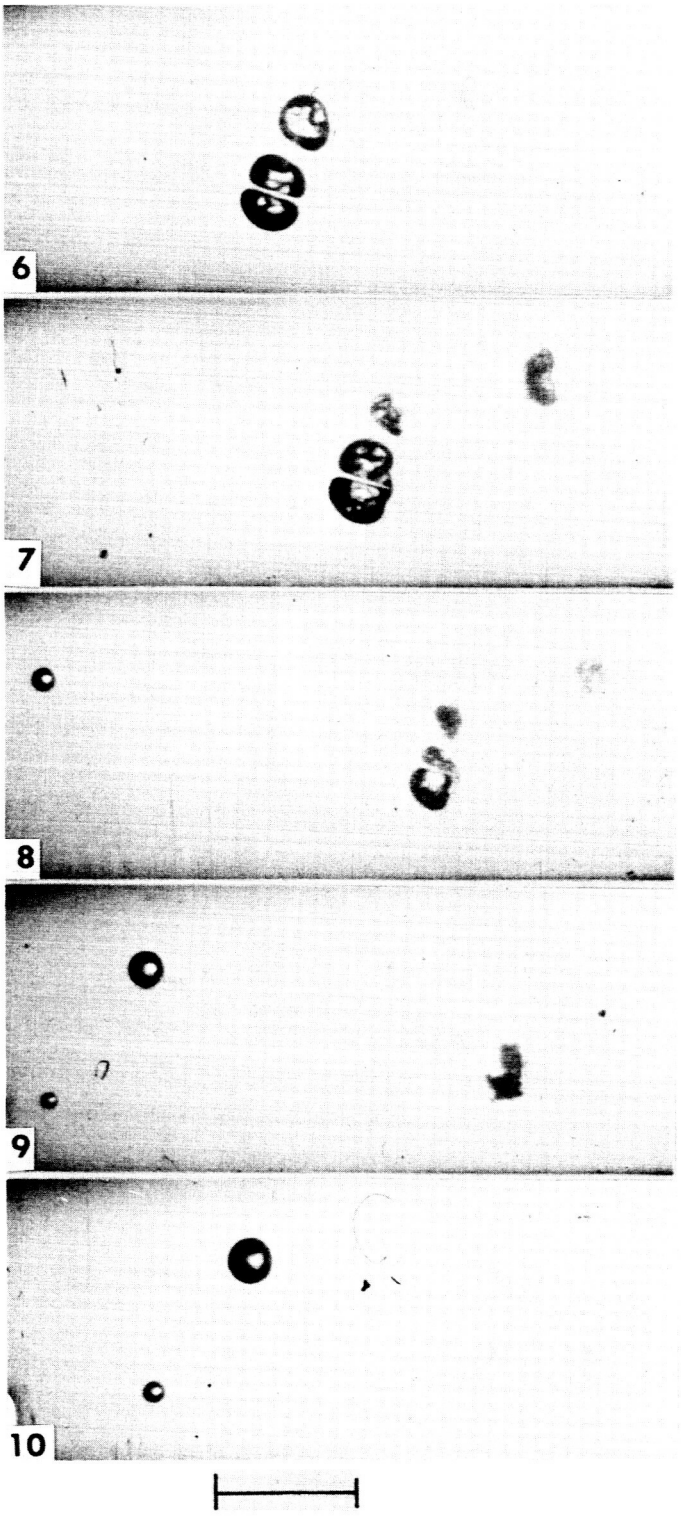

Figure 7. (Continued)

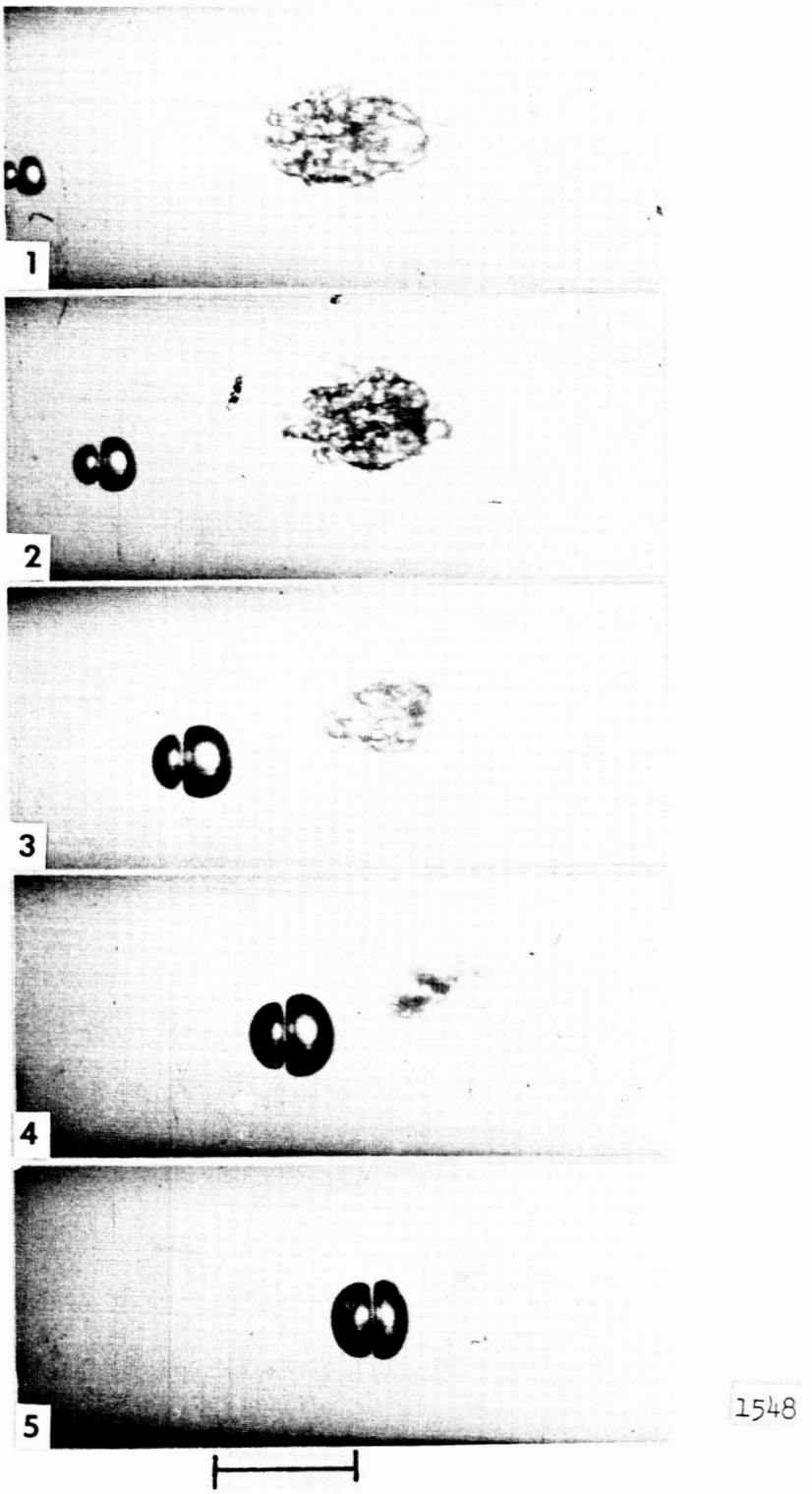

Figure 8. High Speed Photographs, 1/4 inch Venturi Throat, Velocity 74.6 ft/sec, Air Content 2.35 vol. %, 150 Microseconds per Frame, Scale Length 0.25 in.

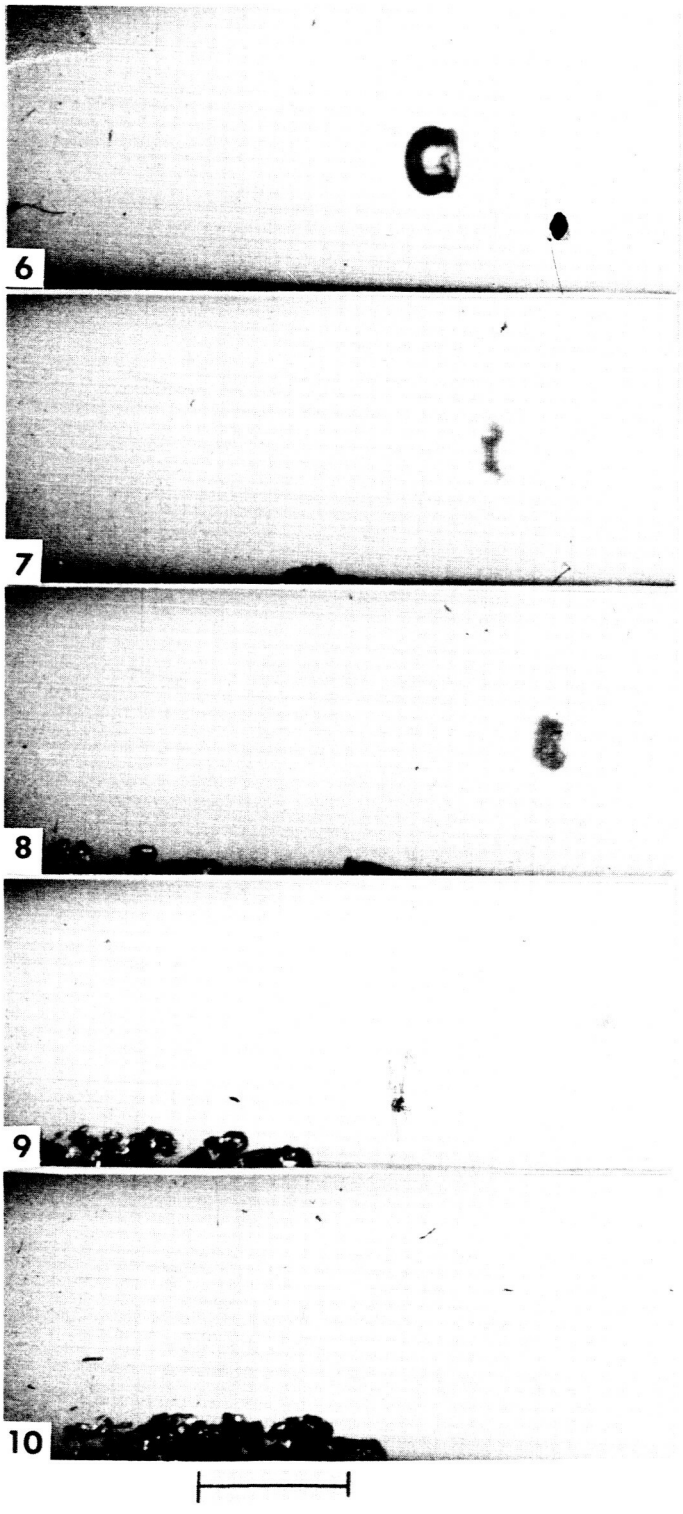

Figure 8. (Continued)

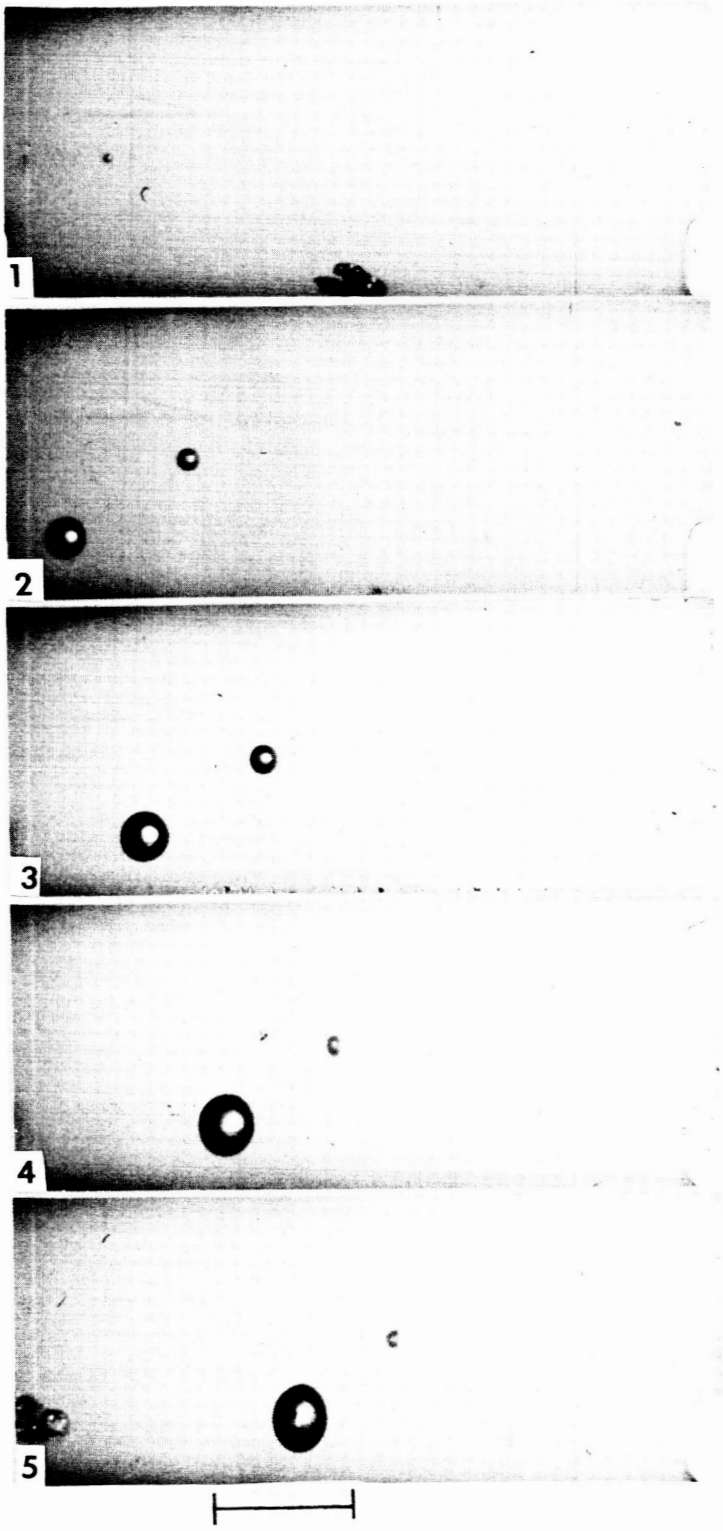

Figure 9. High Speed Photographs, 1/4 inch Venturi Throat, Velocity 74.6 ft/sec, Air Content 2.35 vol. %, 132 Microseconds per Frame, Scale Length 0.25 in.

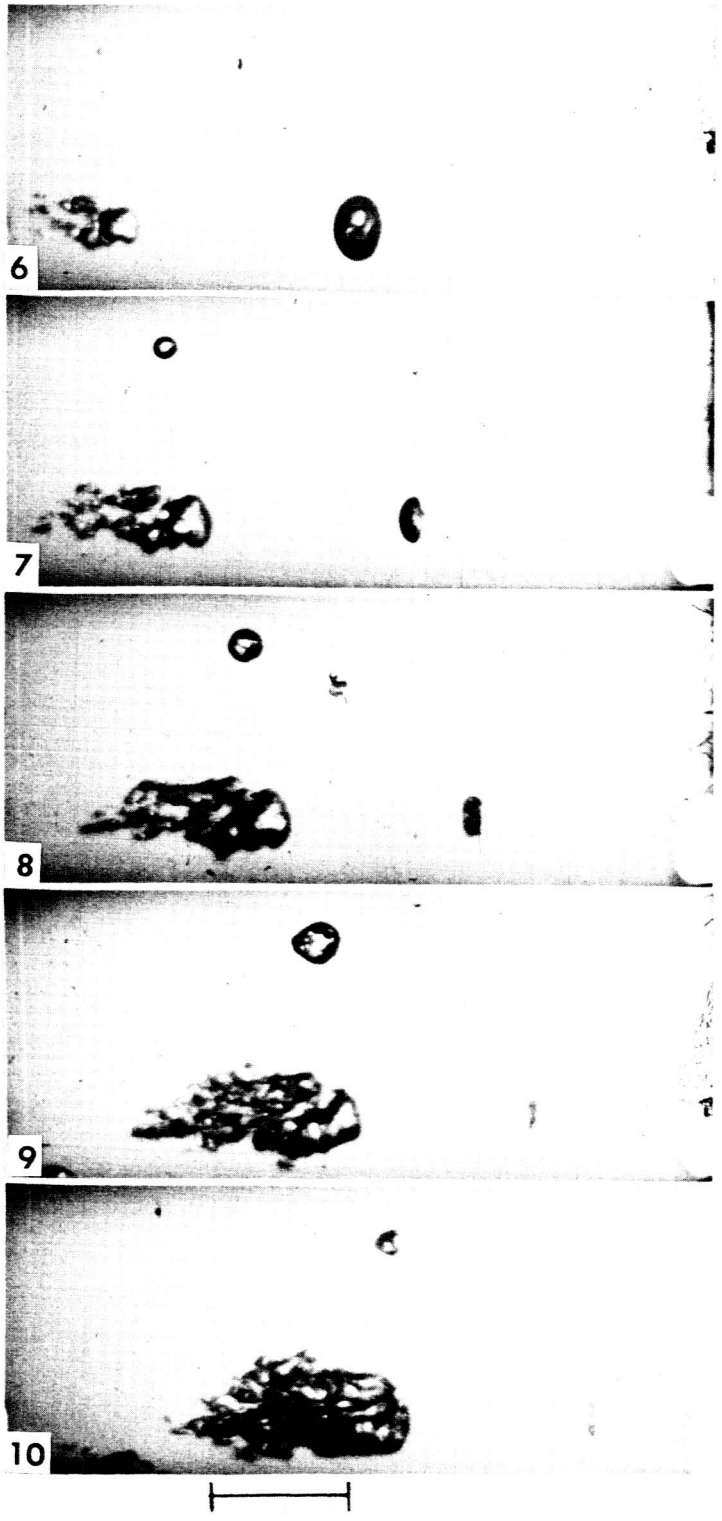

Figure 9. (Continued)

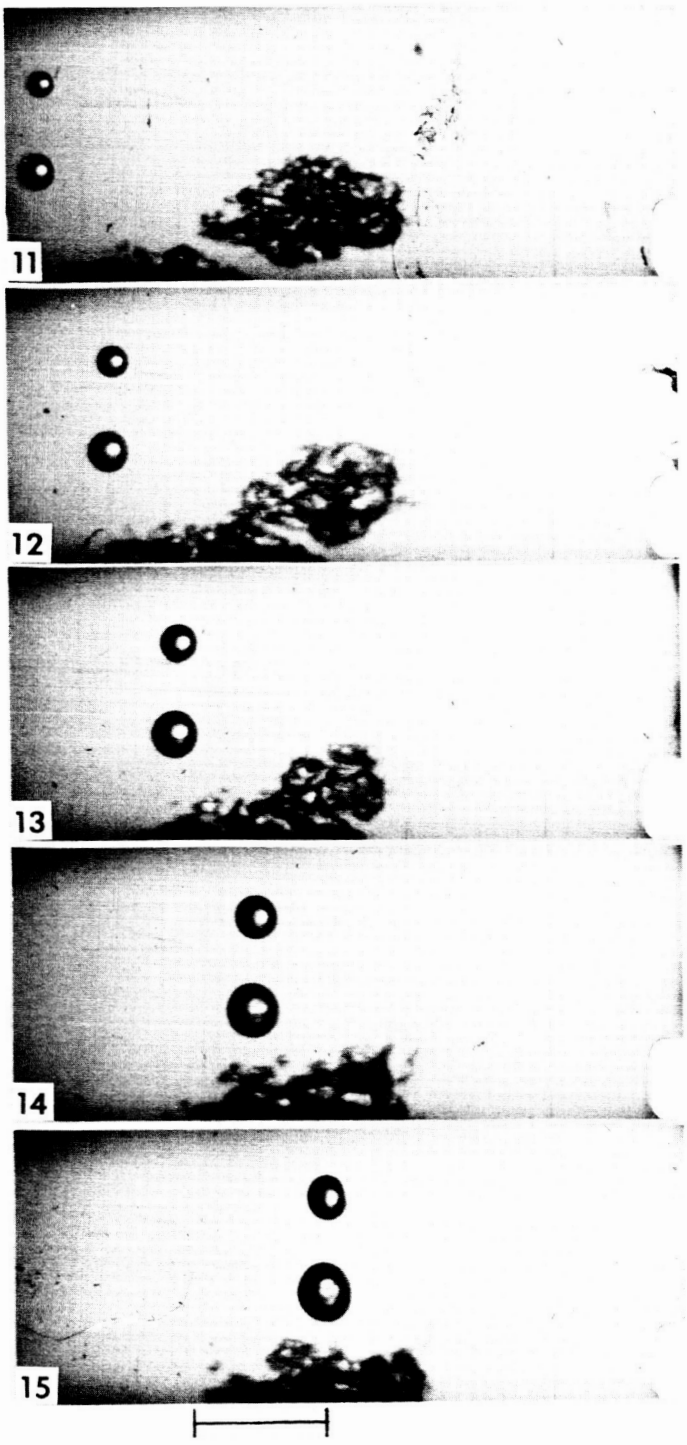

Figure 9. (Continued)

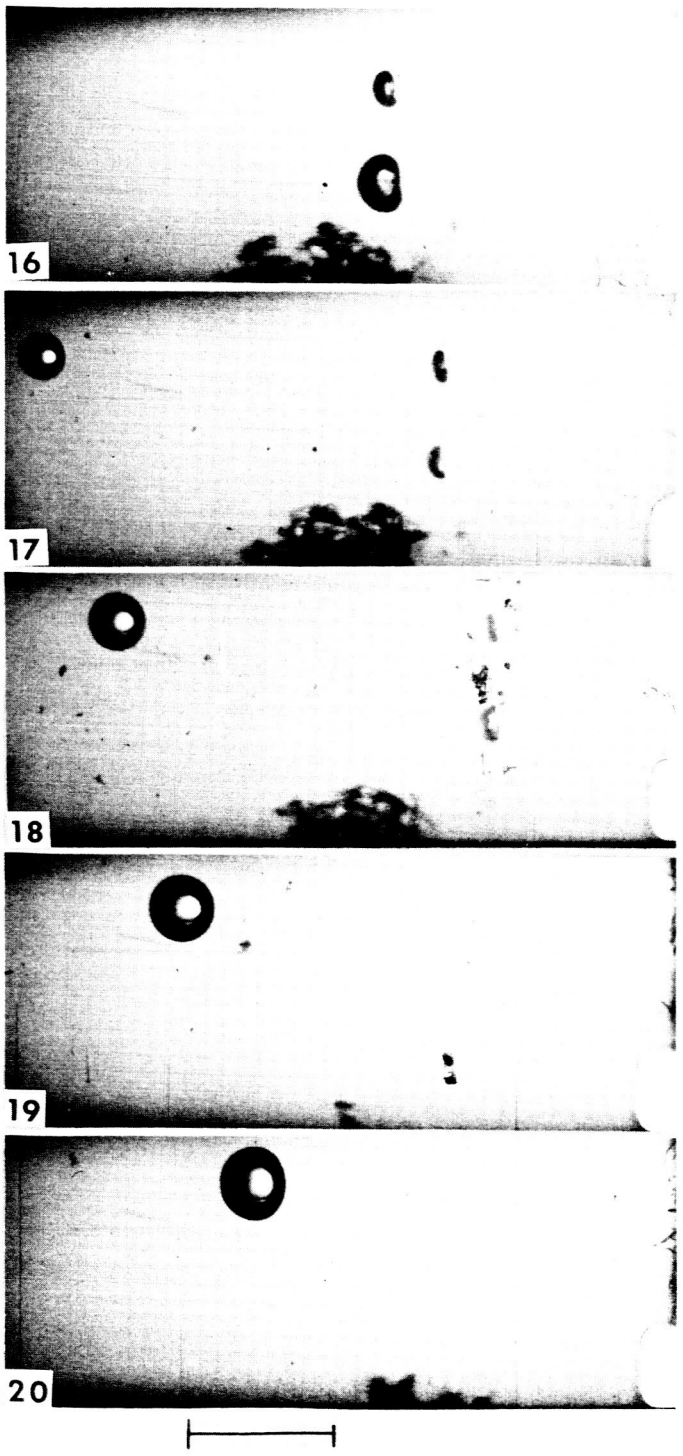

Figure 9. (Continued)

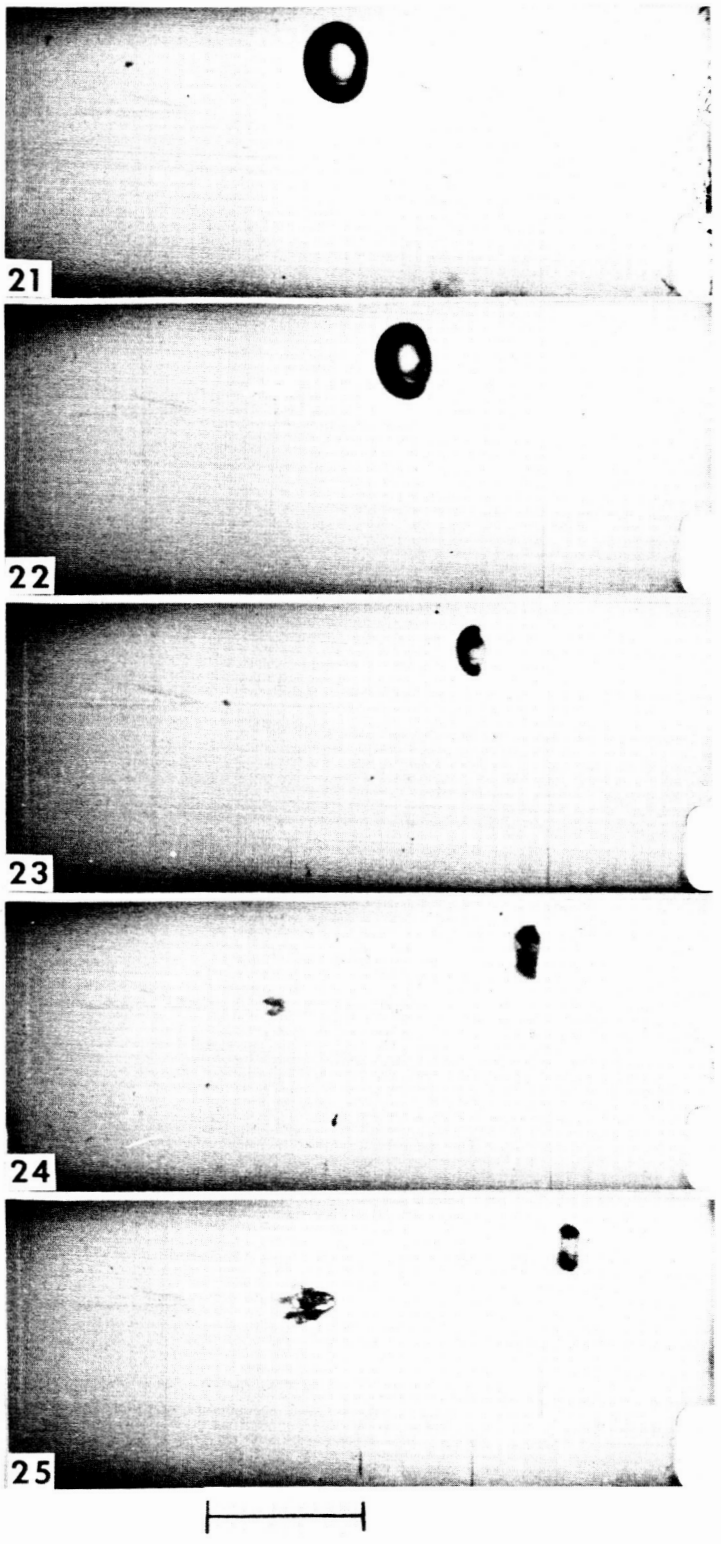

Figure 9. (Continued)

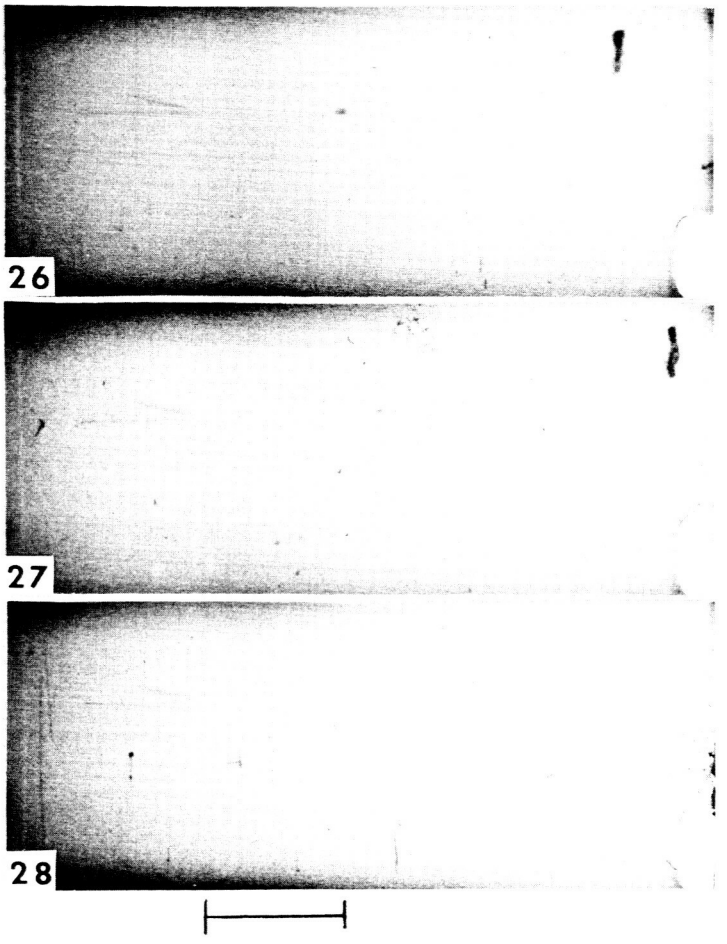

Figure 9. (Continued)

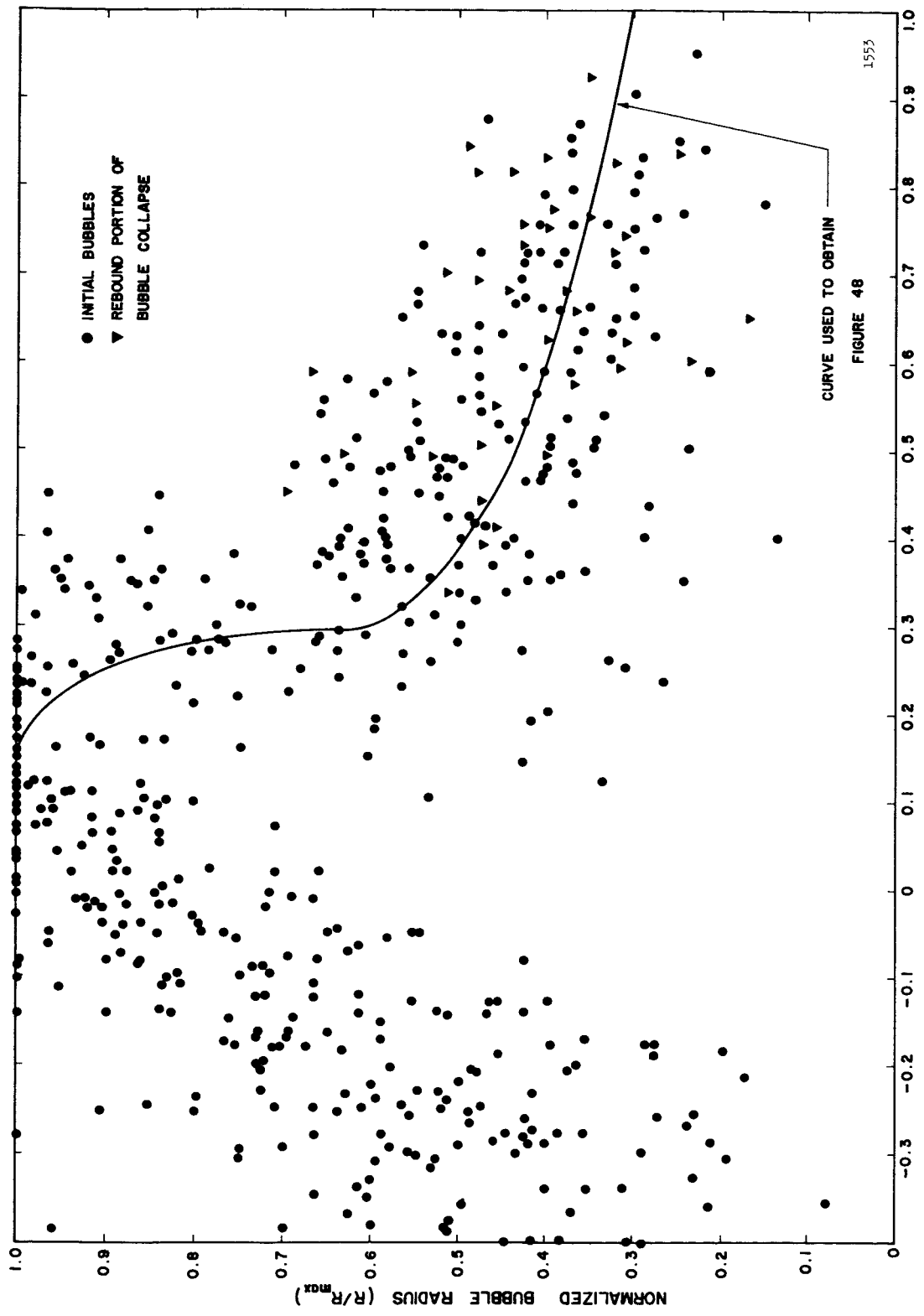

Figure 10. Normalized Observed Bubble Radius vs Distance from Throat Exit, 73 Bubbles

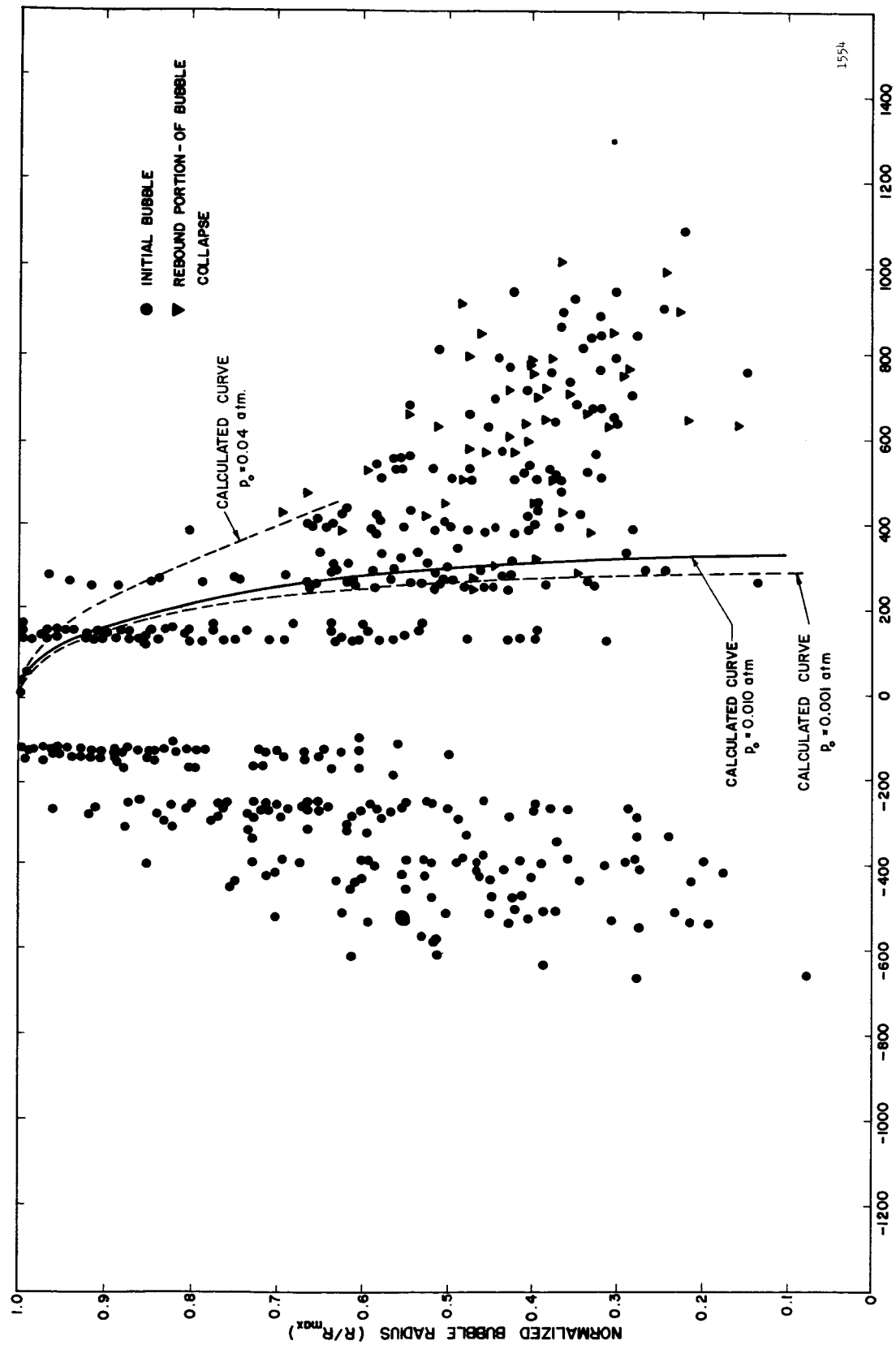

Figure 11. Normalized Observed Bubble Radius vs Time from the First Observed Maximum Radius, 73 Bubbles